Transactions of the Materials Research Society of Japan 31[1] 15-18 (2006)

Electronic Structure in the Valence Band of *C*-axis Oriented $Sr_{0.5}Ba_{0.5}Nb_2O_6$ Thin Film on $La_{0.05}Sr_{0.95}TiO_3$ Substrate

Yoshiki Ebina, Tohru Higuchi, Takeshi Hattori and Takeyo Tsukamoto
Department of Applied Physics, Tokyo University of Science, 1-3 Kagurazaka, Shinjuku, Tokyo 162-8601, Japan
Fax: 81-3-5228-8241, e-mail: higuchi@rs.kagu.tus.ac.jp

The $Sr_{0.5}Ba_{0.5}Nb_2O_6$ thin films on $La_{0.05}Sr_{0.95}TiO_3$ substrates were prepared by pulsed laser deposition. When the substrate temperature and oxygen gas pressure were fixed at 750°C and 7.5 mTorr, respectively, the SBN thin film exhibited a strongly *c*-axis orientation and a smooth surface. The $Sr_{0.5}Ba_{0.5}Nb_2O_6$ thin film consisted of well-developed grains with a diameter of 200 nm. Its remanent polarization (P_r) and coercive field (E_c) were $2P_r$=32.1 μC/cm^2 and $2E_c$=135 kV/cm, respectively. The valence band is mainly composed of the O 2*p* state hybridized with Nb 4*d* state. The contribution of Nb 4*d* partial density of state, which is estimated from the rate of total density of state, was approximately 20 % in the valence band.

Key words: $Sr_{0.5}Ba_{0.5}Nb_2O_6$ thin film, pulsed laser deposition, ferroelectricity, hybridization effect, electronic structure

1. INTRODUCTION

$Sr_{1-x}Ba_xNb_2O_6$ has a tetragonal unfilled tungsten bronze structure and is built by Nb-O octahedral linked by their corners in such a way that three different types of channels are formed along the tetragonal c-axis. One channel is always empty, the second is partially filled only by Sr atoms, while the third one is also partially occupied by Sr and Ba. The distribution of Sr and Ba atoms in the channels depends on the composition of the compound, which will be henceforth characterized by the Sr fraction x of the crystal throughout the article. The $Sr_{1-x}Ba_xNb_2O_6$ is widely studied ferroelectric relaxor crystal with a high potential for applications due to its large electro-optic, pyroelectric, and piezoelectric coefficients. Therefore, the ferroelectric and structural properties have been studied in single crystal form.

The $Sr_{1-x}Ba_xNb_2O_6$ thin films have been prepared by several fabrication techniques, such as sol-gel, pulsed laser deposition (PLD) and chemical solution deposition [2-10]. The *c*-axis orientation of the thin films has been already obtained at $SrTiO_3$ and MgO substrate [2-8]. In recent years, Sakamoto et al. has reported that the Gd, Er-doped $BaNb_2O_6$ thin films on Pt/MgO substrate exhibits a prominent *c*-axis preferred orientation and has a remanent polarization (P_r) of 7.0 mC/cm^2 [9-10], although the effect of leakage current is included. However, the details of ferroelectric and structural properties of $Sr_{1-x}Ba_xNb_2O_6$ thin film have not been reported thus far.

In this study, the *c*-axis oriented $Sr_{1-x}Ba_xNb_2O_6$ thin films were prepared on $La_{0.05}Sr_{0.95}TiO_3$ (LSTO) substrates by pulsed laser deposition (PLD). The lattice mismatch between $Sr_{1-x}Ba_xNb_2O_6$ and LSTO was estimated to be approximately 5.0 %. Furthermore, the electronic structure is also measured by soft-X-ray emission spectroscopy (SXES) and X-ray absorption spectroscopy (XAS). SXES and XAS reflect the electronic structures of valence band and conduction band, respectively. In this paper, we discuss about the relationship between ferroelectricity and electronic structure of $Sr_{1-x}Ba_xNb_2O_6$ thin film.

2. EXPERIMENTAL

$Sr_{1-x}Ba_xNb_2O_6$ thin films were deposited on a (100)-oriented LSTO substrate by PLD using a $Sr_{1-x}Ba_xNb_2O_6$ ceramic target. The single crystals of LSTO substrates, which were grown by the Czochralski method, were obtained from Furuuchi Kagaku Co., Ltd. The SBN ceramic target was prepared as follows: $SrCO_3$, $BaCO_3$ and Nb_2O_5 powders were mixed at a cation molar ratio of Sr:Ba:Nb = 0.5:0.5:2 using a wet ball mill. The mixture was pressed into a disk shape at 100kN and sintered for 4h at 1300°C. The target disk was polished to 21.3mm diameter and 4mm thickness. The target was examined using X-ray diffraction (XRD). The density of SBN ceramic target was approximately 94 %.

The PLD system was arranged in a symmetric configuration with a rotating substrate holder for compositional uniformity. The base pressure was ordinarily 9.0×10^{-9} Torr, and the substrate was inserted from a load lock chamber to maintain a low base pressure. A KrF excimer laser (λ= 248 nm) was used for the ablation of the target. The laser power density and repetition frequency were 220 mJ/cm^2 and 9 Hz, respectively. The film thickness was fixed at approximately 400 nm. The top Pt electrodes with a diameter of 0.2mm were deposited on the film surface through a metal shadow mask by rf magnetron sputtering.

The structural properties were characterized by XRD analysis. The surface morphologies were observed by atomic-force-microscopy (AFM). The ferroelectricity was characterized using the ferroelectric property measurement system RT-6000HVS.

The electronic structure was characterized by SXES and XAS, which determine the electronic structure in the bulk state. The SXES and XAS were carried out in the revolver undulator beamline BL-19B at the Photon

Factory of the High-Energy Accelerator Organization, Tsukuba, Japan. Synchrotron radiation was monochromatized using a varied-line spacing plain grating whose average groove density was 1000 lines/mm. The SXES spectrum was measured using a soft-X-ray emission spectrometer. The XAS spectrum was measured using a Si photodiode. The energy resolutions of SXES and XAS were approximately 0.4 eV and 0.1 eV, resepctively.

3. RESULTS AND DISCUSSION

Figure 1 shows the XRD patterns as a function of the substrate temperature (T_{sub}) for the $Sr_{0.5}Ba_{0.5}Nb_2O_6$ thin films. The oxygen gas pressure during the deposition was fixed at 7.5 mTorr. The (100) and (200) peaks of the LSTO substrates are observed at 2θ=22.8° and 46.7°, respectively. The $Sr_{0.5}Ba_{0.5}Nb_2O_6$ thin films prepared at T_{sub}=700 and 800°C do not exhibit the (001), (002) and (410) peaks. This originates the low crystallization and oxygen vacancies. The (001) and (002) peaks of the $Sr_{0.5}Ba_{0.5}Nb_2O_6$ thin films prepared at T_{sub}=750°C are observed at 2θ=22.2° and 46.0°, respectively. Thus, the SBN thin film prepared at 750°C exhibits a strong *c*-axis orientation.

Figure 2 shows the AFM image of the highly *c*-axis oriented $Sr_{0.5}Ba_{0.5}Nb_2O_6$ thin film prepared at T_{sub}=750°C. The $Sr_{0.5}Ba_{0.5}Nb_2O_6$ thin film consisted of well-developed grains with a diameter of 200 nm. Its surface roughness was approximately 20 nm against a film thickness of 400 nm. The $Sr_{0.5}Ba_{0.5}Nb_2O_6$ thin film was epitaxially growth with a *c*-axis perpendicular to the LSTO substrate.

Figure 3 shows the hysteresis loops as a function of T_{sub} for the SBN thin films. The as-deposited $Sr_{0.5}Ba_{0.5}Nb_2O_6$ thin films did not exhibit ferroelectricity. Therefore, the as-deposited $Sr_{0.5}Ba_{0.5}Nb_2O_6$ thin films were annealed at 700~800°C in oxygen atmosphere for 1 h in order to investigate the effect of postannealing. The $Sr_{0.5}Ba_{0.5}Nb_2O_6$ thin film deposited at T_{sub}=700°C do not also exhibit ferroelectricity due to poor crystallization, as shown in Fig. 2. The SBN thin film deposited at T_{sub}=800°C is uniquely shape, which contributes to the large leakage current (>10^{-4} A/cm^2). A good *P-E* hysteresis loop of the $Sr_{0.5}Ba_{0.5}Nb_2O_6$ thin film is observed at T_{sub}=775°C. Then, the P_r and coercive field (E_c) were $2P_r$=32.1 μC/cm^2 and $2E_c$=135 kV/cm, respectively. The ε was approximately 160. These values are superior to those of the $Sr_{0.5}Ba_{0.5}Nb_2O_6$ thin films obtained by sol-gel and chemical solution deposition methods [6-11]. The good ferroelectricity of the highly *c*-axis oriented $Sr_{0.5}Ba_{0.5}Nb_2O_6$ thin film at T_{sub}=775°C contributes to the relatively small grain size and the smooth surface, as shown in Fig. 2.

Figure 4 shows the O 1*s* X-ray absorption (XAS) spectrum of $Sr_{0.5}Ba_{0.5}Nb_2O_6$ thin film. From the dipole selection rule, it is understood that the O 1s XAS spectrum of the 4*d* transition metal oxide corresponds to the transition from O 1*s* to O 2*p* character hybridized into the unoccupied metal 4*d* states. The broad band at around 535 eV is attributed to the Sr 4*d* and Ba 5*d* bands that are mixed with unoccupied O 2*p* character. The peak at around 530 eV is the t_{2g}-subband of the Nb 4*d* states: the e_g-subband is considered to be obscured by

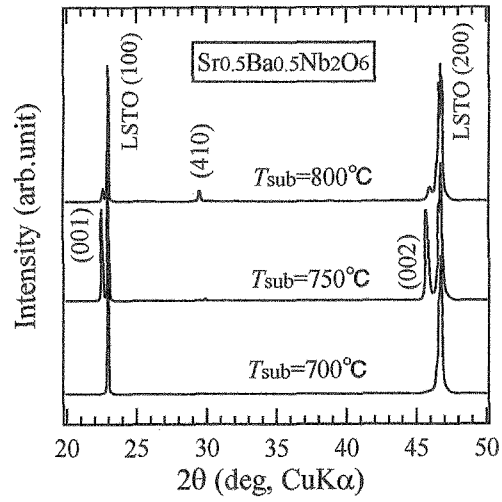

Fig. 1: XRD patterns as a function of T_{sub} in $Sr_{0.5}Ba_{0.5}Nb_2O_6$ thin films.

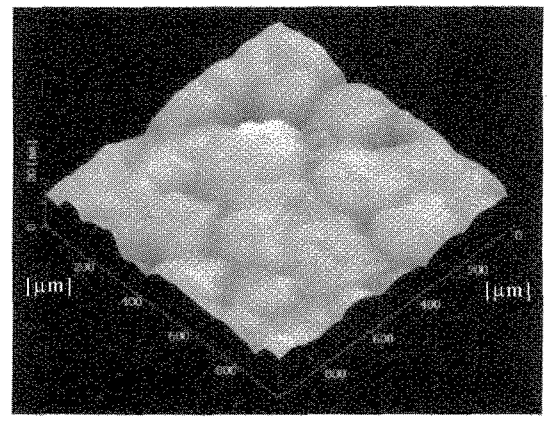

Fig. 2: AFM image of $Sr_{0.5}Ba_{0.5}Nb_2O_6$ thin film deposited at T_{sub}=750°C.

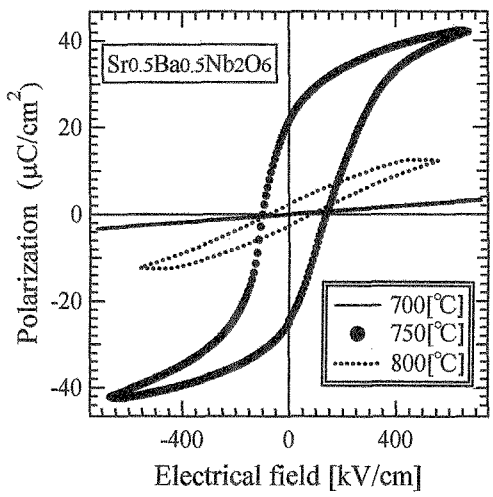

Fig. 3: *P-E* hysteresis loops as a function of T_{sub} in $Sr_{0.5}Ba_{0.5}Nb_2O_6$ thin films.

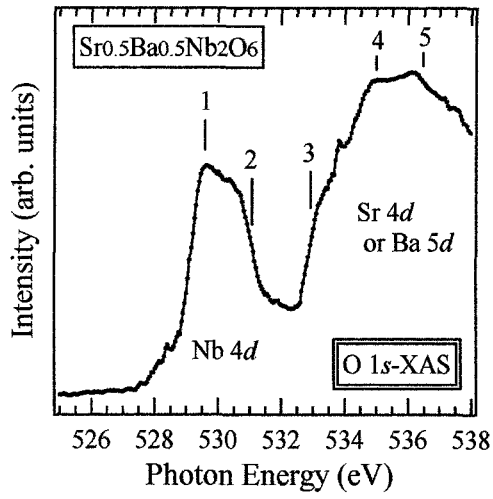

Fig. 4: O 1s XAS spectrum of $Sr_{0.5}Ba_{0.5}Nb_2O_6$ thin film. The numbers indicate the photon energies at which the resonant-SXES spectra were measured.

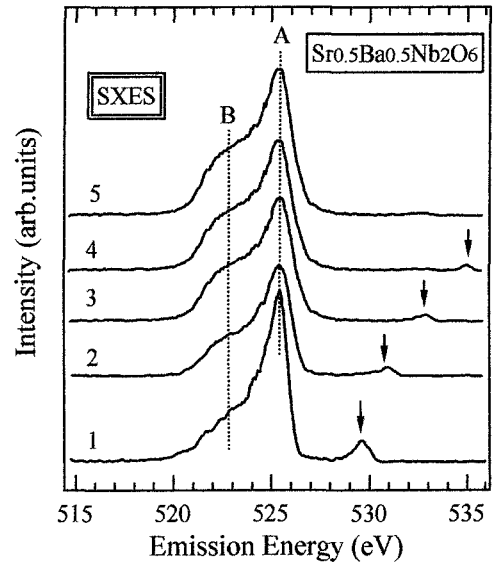

Fig. 5: O 1*s* SXES spectra of $Sr_{0.5}Ba_{0.5}Nb_2O_6$ thin film excited at various photon energies indicated in Fig. 4. Arrows show the energy positions of the excitation photon energies.

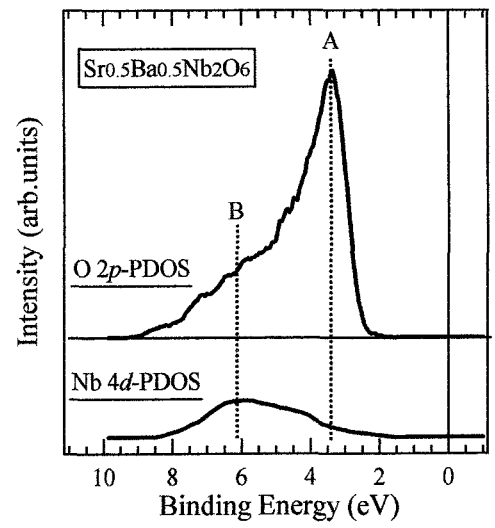

Fig. 6: Comparison of O 1*s* and Nb 4*p* SXES spectra in the valence band region of $Sr_{0.5}Ba_{0.5}Nb_2O_6$ thin film. The O 1*s* SXES spectrum is spectrum 1 in Fig. 5.

the overlapping Sr 4*d* or Ba 5*d* band. The vertical bars, which are labeled from 1 to 5, indicate the selected photon energies from the resonant SXES measurements.

Figure 5 shows the O 1s resonant-SXES spectra of $Sr_{0.5}Ba_{0.5}Nb_2O_6$ thin film. The clear selection rule of SXES is caused mainly within the same atomic species, because the core hole is strongly localized. For this reason, the O 1*s* SXES spectra reflect the O 2*p* PDOS. The obtained O 2*p* PDOS corresponds to the band structure in the valence band region, since the valence band of $Sr_{0.5}Ba_{0.5}Nb_2O_6$ is mainly composed of O 2*p*. An arrow shown each spectrum indicates the elastic scattering of excitation photon. Two features denoted by A and B are observed at ~525.5 eV and ~522.7 eV, respectively. Except for the spectrum 1, the intensities of the features A and B increase slightly with increasing excitation photon energy since the numbers of electrons excited to the conduction band from the O 1*s* core level increase with excitation photon energy, as shown in Fig. 1(a). On the other hand, the intensity of the feature A of the spectrum 1 is stronger than those of other spectra. This indicates that the O 1*s* → 2*p* resonance effect occurs at the t_{2g}-absorption peak of Fig. 4. However, the O 1*s* resonant-SXES spectra reflect the O 2*p* fluorescence component in the valence band region because the existences of soft-X-ray Raman scattering and new structure with excitation photon, which is often useful observing in resonant-SXES spectra excited at transition metal sites, are not found in these spectra. Therefore, the hybridization effect between Nb 4*d* and O 2*p* states in the valence band region can discuss quantitatively from the SXES spectra.

Figure 6 shows the Nb 4*p* and O 1*s* SXES spectra in the valence band region of $Sr_{0.5}Ba_{0.5}Nb_2O_6$ thin film. The intensity of each spectrum is normalized by the beam current and measurement time. The O 1*s* SXES spectrum, which reflects the O 2*p*-PDOS, exhibited the spectrum 2 corresponding to non-resonance in Fig. 1(b) because the spectrum 1 corresponding to on-resonance does not reflect the true DOS. The Nb 4*p* SXES measured at $h\nu$=65 eV reflects the Nb 4*d*-PDOS in the valence band region. The contributions of Sr 4*d* and Ba 5*d* were not observed in the valence band region. Thus, the sum of O 2*p* PDOS and Nb 4*d* PDOS is total DOS in the valence band of $Sr_{0.5}Ba_{0.5}Nb_2O_6$ thin film.

The Nb 4*d*-PDOS has broad distribution on the feature B side. The Nb 4*d* contribution is more significant in the higher binding energy (feature B), where the O 2*p* states have a larger admixture of Nb 4*d* states. This shows that the indispensable magnitudes mix with the valence state. In other words, the valence states originating from the O 2*p* states are hybridized with the Nb 4*d* states. From the distributions of Nb 4*d* and O 2*p*-PDOS, we can estimate that the feature A

corresponds to the nonbonding state and the feature B corresponds to the bonding state that is well mixed with Nb 4*d* state. The hybridization effect between the Nb 4*d* and O 2*p* states in Nb oxide has not been reported thus far. However, similar hybridization effect has been observed in $4d^0$ metal transition oxides such as ZrO_2 and $CaZrO_3$ [12,13]. In perovskite-type oxide $CaZrO_3$, it was reported that the contribution of Zr 4*d*-PDOS is more significant in the higher binding energy side in the valence band region, where the bonding O 2*p* states have a larger admixture of Zr 4*d* states. The contribution of Zr 4*d*-PDOS has been reported to be approximately 25 % in the valence band [13]. For $Sr_{0.5}Ba_{0.5}Nb_2O_6$ thin film, the contribution of Nb 4*d*-PDOS, which is estimated from the rate of total DOS, was about 20 % in the valence band.

4. CONCLUSION

We prepared the highly *c*-axis oriented $Sr_{0.5}Ba_{0.5}Nb_2O_6$ thin film on LSTO substrate by PLD method and studied its electronic structure using SXES and XAS. When the Po_2 and T_{sub} were fixed at 7.5 mTorr and 750°C, respectively, the $Sr_{0.5}Ba_{0.5}Nb_2O_6$ thin film exhibited a highly *c*-axis oriented $Sr_{0.5}Ba_{0.5}Nb_2O_6$ single phase. The *c*-axis oriented $Sr_{0.5}Ba_{0.5}Nb_2O_6$ thin film consisted of well-developed grains and exhibited a good *P-E* hysteresis loop. Then, P_r and E_c were $2P_r$=32.1 μC/cm^2 and $2E_c$=135 kV/cm, respectively. The O 1*s* and Nb 4*p* SXES spectra exhibited the O 2*p* PDOS and Nb 4*d* PDOS, respectively, in the valence band. The energy position of the O 2*p* state overlaps with that of the Nb 4*d* state, indicating that the O 2*p* state hybridizes with the Nb 4*d* state in the valence band. The contribution of the Nb 4*d* PDOS to the total DOS was estimated to be approximately 20% in the valence band.

ACKNOWLEDGEMENT

We would like to thank Mr. M. Sogawa for his useful discussion. This work was supported by a Grant-In-Aid for Scientific Research from the Ministry of Education, Culture, Sports, Science and Technology.

REFERENCES

[1] P. B. Jamieson, S. C. Abrahams and J. L. Bernstein: J. Chem. Phys. **48** (1968) 5048.
[2] C. J. Chen, Y. Xu, R. Xu and J. D. Mackenzie: J. Appl. Phys. **69** (1991) 1763.
[3] S. Hirano, T. Yogo, K. Kikuta and K. Ogiso: J. Am. Ceram. Soc. **75** (1992) 1697.
[4] K. Tanaka, O. Nakagawa, M. Nakano, T. Shimuta, H. Tabata and T. Kawai: Jpn. J. Appl. Phys. **37** (1998) 6142.
[5] M. Nakano, H. Tabata, K. Tanaka, Y. Katayama and T. Kawai: Jpn. J. Appl. Phys. **36** (1997) L1331.
[6] S. S. Thony, K. E. Youden, J. S. Harris and L. Hesselink: Appl. Phys. Lett. **65** (1994) 2018.
[7] W. J. Lin, T. Y. Tseng, S. P. Lin, S. L. Tu, S. J. Yang, J. J. Harn, K. S. Liu and I. N. Lin: Jpn. J. Appl. Phys. **34** (1995) L625.
[8] H. F. Cheng, C. T. Hu and I. N.Lin: Jpn. J. Appl. Phys. **36** (1997) 284.
[9] W. Sakamoto, Y. Horie, T. Yogo and S. Hirano: Jpn. J. Appl. Phys. **40** (2001) 5599.
[10] W. Sakamoto, M. Mizuno, T. Yamaguchi, K. Kikuta and S. Hirano: Jpn. J. Appl. Phys. **42** (2003) 5913.
[11] N. Ohtake, T. Higuchi, K. Ando, A. Fukishima, S. Shin and T. Tsukamoto: Jpn. J. Appl. Phys. **43** (2004) 7627.
[12] T. Higuchi, T. Tsukamoto, Y. Tezuka, K. Kobayashi, S. Yamaguchi and S. Shin: Jpn. J. Appl. Phys. **39** (2000) L133.
[13] C. Morant, A. Fernandez, A. R. Gonzalez-Elipe, L. Soriano, A. Stampfl, A. N. Bradshaw and I. M. Sanz: Phys. Rev. B **52** (1995) 11711.

(Received December 10, 2005; Accepted January 31, 2006)